Chemistry–A European Journal
Research Article
doi.org/10.1002/chem.202300946
Chemistry Europe
European Chemical Societies Publishing
www.chemeurj.org

VIP *Very Important Paper*

Towards Fast Circularly Polarized Luminescence in 2-Coordinate Chiral Mechanochromic Copper(I) Carbene Complexes

André M. T. Muthig,[a] Justin Wieland,[a] Carsten Lenczyk,[a] Stefan Koop,[a] Jacopo Tessarolo,[a] Guido H. Clever,[a] Benjamin Hupp,[a] and Andreas Steffen*[a]

A series of chiral mechanochromic copper(I) cAAC (cAAC = cyclic (alkyl)(amino)carbene) complexes with a variety of amide ligands have been studied with regard to their photophysical and chiroptical properties to elucidate structure-property relationships for the design of efficient triplet exciton emitters exhibiting circularly polarized luminescence. Depending on the environment, which determines the excited state energies, either thermally activated delayed fluorescence (TADF) from $^{1/3}$LLCT states or phosphorescence from ^{3}LLCT/LC states occurs. However, neither chiral moieties at the carbene nor at the carbazolate ligands provide detectable luminescence dissymmetries g_{lum}. An exception is [Cu(phenoxazinyl)(cAAC)], showing orange to deep red TADF with λ_{max} = 601–715 nm in solution, powders and in PMMA. In this case, the amide ligand can undergo distortions in the excited state. This design motif leads to the first linear, non-aggregated CPL-active copper(I) complex with g_{lum} of $-3.4\cdot10^{-3}$ combined with a high radiative rate constant of $6.7\cdot10^{5}$ s^{-1}.

Introduction

Circularly polarized luminescence (CPL) is a favorable tool for a variety of applications, including quantum computing,[1] cryptography,[2] spintronics,[3] chemical sensors,[4] biological probes[5] and display technologies.[6] The efficiency of a chiral molecular emitter for generating CPL with a defined handedness, i.e. the emission excess of photons with a spin-angular momentum of $J_z = \pm 1$, is typically quantified by the anisotropy factor g_{lum} and can reach maximum values of ± 2, corresponding to purely left- or righthanded light, respectively. It is important to note that the dissymmetry of the radiative transition depends on the relative magnitudes of the electronic $(\vec{\mu})$ and magnetic $(\vec{m})$ transition dipole moment vectors, and the angle θ between them (Eq. (1)).[7]

$$g = \frac{4\cdot\left|\vec{\mu}\right|\left|\vec{m}\right|\cos(\theta)}{\left|\vec{\mu}\right|^2+\left|\vec{m}\right|^2} \quad (1)$$

Bearing in mind that $\vec{m}$ is often several orders of magnitude smaller than $\vec{\mu}$, and that the latter determines the radiative rate constant k_r, it becomes obvious that only electronic dipole forbidden transitions in chiral molecules can provide access to CPL. For example, high g_{lum} values >1 have been reported for Laporte-forbidden f-f* transitions in lanthanide complexes,[8] while d-d* transitions in chiral octahedral Cr^{III} compounds can exhibit g_{lum} of up to 0.2.[9] However, implementation of these classes of CPL emitters in electrically driven luminescence applications that require triplet exciton emission, for example OLEDs, would lead to serious efficiency roll-offs and small external quantum efficiencies (EQE) due to their very low $k_P <$ 50 s^{-1} for phosphorescence.[10] Archetypical molecular OLED emitters of the 4d and 5d elements have been found to display high k_P of 10^4–10^6 s^{-1},[11] but the dissymmetry factors g_{lum} of the majority of their chiral examples usually do not reach beyond $g_{lum} = 10^{-4}$–10^{-3}.[12] The only exception that we are aware of, showing remarkable g_{lum} of up to $1\cdot10^{-2}$ combined with moderate k_p of 10^3–10^4 s^{-1}, is a family of chiral Pt^{II}-based complexes bearing helicene-type ligands.[13]

An interesting approach to bypass the dilemma of sacrificing a high k_r of triplet state emission for sufficiently high luminescence dissymmetries g_{lum} suitable for device applications would be the investigation of chiral thermally activated delayed fluorescence (TADF) emitters.[14] In contrast to spin-forbidden $T_1 \rightarrow S_0$ phosphorescence, this mechanism involves endothermic reverse intersystem crossing (rISC) $T_1 \rightarrow S_1$ with subsequent spin-allowed $S_1 \rightarrow S_0$ fluorescence. Although chiral luminophores with a high g_{lum} would exhibit low $\vec{\mu}$ for fluorescence, CP-TADF emission would still be faster than CP phosphorescence directly from T_1.

Various organic TADF emitters with chiral moieties or axial chirality have been studied and a few examples show g_{lum} of up to $1.8\cdot10^{-2}$.[15] Interestingly, the chiroptical properties of the

[a] A. M. T. Muthig, J. Wieland, C. Lenczyk, S. Koop, Dr. J. Tessarolo, Prof. Dr. G. H. Clever, Dr. B. Hupp, Prof. Dr. A. Steffen
Department of Chemistry and Chemical Biology
TU Dortmund University
Otto-Hahn-Str. 6, 44227 Dortmund (Germany)
E-mail: andreas.steffen@tu-dortmund.de

Supporting information for this article is available on the WWW under https://doi.org/10.1002/chem.202300946

fastest molecular TADF emitters to date with k_{TADF} reaching 10^5–10^6 s^{-1}, namely carbene coinage metal amides (CMA),[16–19,20] have not yet been reported. These linearly coordinated donor-M-acceptor (D-M-A, M = Cu, Ag, Au) type compounds exhibit ligand-to-ligand charge-transfer (LLCT) states with some metal-to-ligand (ML)CT admixture, which is most pronounced in copper(I) complexes. Consequently, they can benefit from rotation of the ligands and spin-orbit coupling (SOC) of the d^{10} metal centre, both factors greatly influencing $\Delta E(S_1\text{-}T_1)$ and k_{rISC} to provide high k_{TADF}.[18,21,22] Importantly, the torsion angle between the ligands also has an impact on $\vec{\mu}(S_1 \rightarrow S_0)$, and high-level quantum chemical (QC) calculations showed that k_F in CMAs varies between 10^4 s^{-1} for perpendicular orientation of the ligand planes to 10^7 s^{-1} for a coplanar arrangement.[23] Therefore, the specific structural features of CMA materials should allow control of their chiroptical properties as well. Very recently, Gong et al. discovered for some NHC-based chiral CMAs that their aggregation can give rise to luminescence dissymmetries with g_{lum} of $2.7 \cdot 10^{-2}$ for one very specific single crystalline phase, while in monomers no CPL is observed.[24] However, this aggregation strategy is difficult to transfer into potential device applications.

The potential of molecular transition metal CP-TADF emitters has recently been demonstrated by our study on trigonally coordinated copper(I) carbazolate complexes bearing chiral (S/R)-BINAP ligands, which show efficient TADF with k_r of $3 \cdot 10^5$ s^{-1} combined with high g_{lum} of $\pm 7 \cdot 10^{-3}$ in solution and up to $\pm 2.1 \cdot 10^{-2}$ in the solid state.[25] The efficiency of the TADF process depends on the environment, but careful choice of the matrix materials allowed for successful implementation in CP-OLEDs. Given our long-standing interest in d^{10} coinage metal emitters,[26,27] in particular copper(I) carbene TADF complexes,[17,28] we decided to investigate the chiroptical properties of a series of linearly coordinated [Cu(amide)(cAAC)] complexes (cAAC = cyclic (alkyl)(amino)carbene)) featuring a D-M-A structure with chiral moieties either at the electrophilic carbene ligand or at the amide donor. Although CPL is not detectable for most CMA compounds, we find that [Cu(PZN)(cAAC^{Ment})] (PZN = phenoxazinyl) is an efficient orange-red triplet exciton emitter with high $k_{TADF} = 6.7 \cdot 10^5$ s^{-1} and $g_{lum} = 3.4 \cdot 10^{-3}$ in PMMA films. The hindered ligand rotation in the rigid matrix in combination with a butterfly distortion of the PZN ligand, that is not available to the carbazolate donor ligands, appears to be responsible for the CP-TADF properties of the copper(I) carbene complex.

Results and Discussion

Synthesis and Structural Characterization

The air- and moisture-sensitive chiral copper(I) cAAC amides **1**–**8** were prepared according to an established route by reaction of the corresponding potassium salt of the respective *N*-ligand with [CuCl(cAAC^R)] in THF at RT (Scheme 1).[16,18] While the precursor [CuCl(cAAC^{Me})] is available via the free carbene route,[26] its menthone derivative was obtained by treatment of cAAC^{Ment}·HCl with mesityl copper (see Supporting Information). We isolated **1**–**8** as orange to green powders, which were characterized by multinuclear NMR spectroscopy, elemental analysis and mass spectrometry. However, the 11*H*-benzo[*a*]carbazolate compound **5** turned out to be unstable for further analysis even in the single-crystalline solid state, but its connectivity could be confirmed (Figure S2).

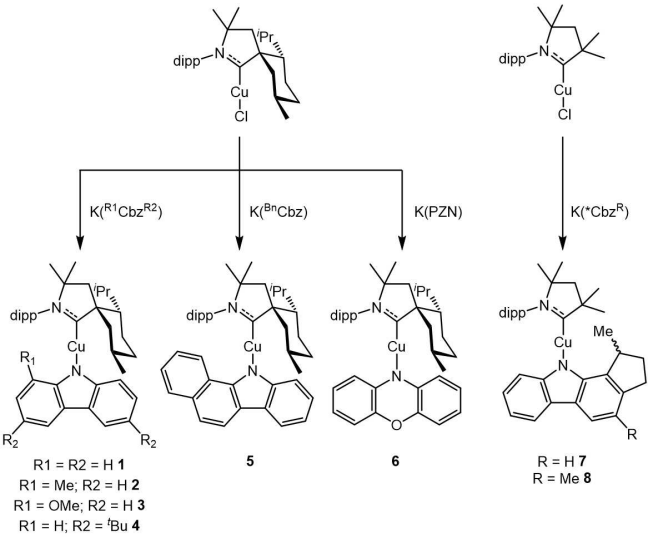

Scheme 1. Synthetic routes towards chiral [Cu(amide)(cAAC^R)] **1**–**8**.

Comparison of the structural information obtained from single crystals of **3** and **6**–**8** suitable for X-ray diffraction analysis shows that a nearly ideal linear coordination geometry is favored (Figure 1 and Table S1). Substitution in the 2-position of the Cbz leads to deviations of the dihedral angle γ between the N-donor and carbene acceptor ligand planes, reaching a maximum of ca. 24° for **7**. As reported for some other d^{10} coinage metal carbazolates, we observe a tilting of the Cbz towards the cAAC that is most pronounced for [Cu(Cbz^{OMe})(cAAC^{Ment})] (**3**) with $\beta = 153.17(9)°$ (Figure 1). The rationale behind these structural peculiarities is not clear and certainly involves electronic and steric effects, such as C-(carbene)-M–N π conjugation and rehybridization of the ipso-*N*, but also packing effects in the solid state.[25] However, as demonstrated by the group of Marian,[14,23] the dihedral angle γ is the most important structural feature determining the efficiency of TADF in such D-M-A compounds.

We note that **6** is less distorted, with $\gamma = 0.4(3)°$ and a butterfly angle between the two aromatic planes of the amide ligand of only $\alpha = 173.43(9)°$, than [Au(PZN)(cAAC^{Ad})] with 160.5(3)° and 21.1(4)° for α and γ, respectively (see below).[18] It is important to note that our NMR studies suggest that free rotation occurs in solution at room temperature, as only half as many signals as expected are found in the ^{1}H and ^{13}C NMR spectra for the symmetrical *N*-donor ligands of **2**, **4** and **6**. An alternative explanation is that the chiral cAAC^{Ment} does not influence the *trans* ligand, however, dynamical rotation processes occurring with low activation barriers at room temperature have previously been reported for structurally related

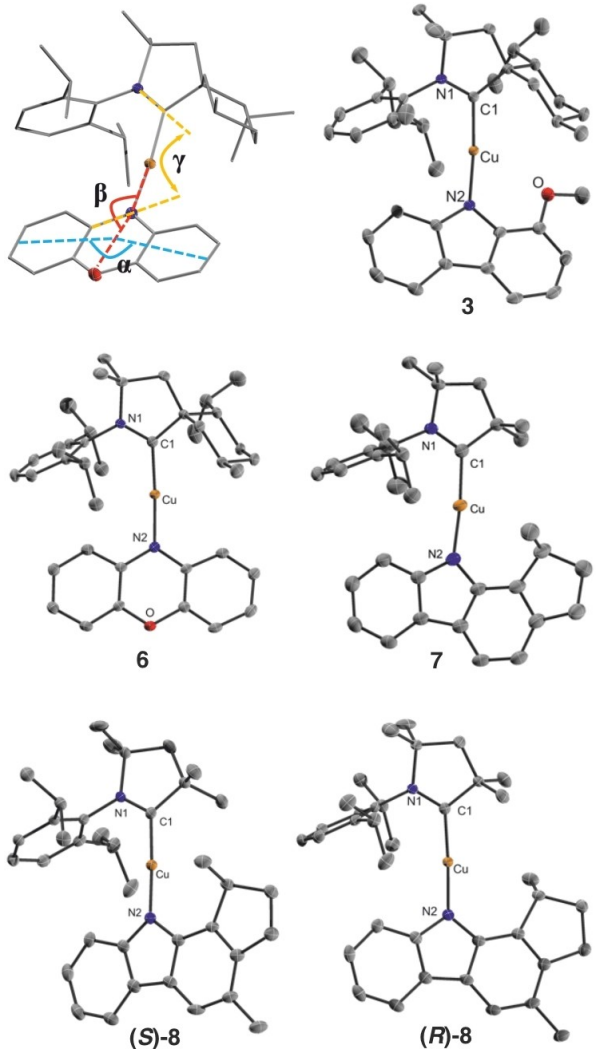

Figure 1. Molecular structures obtained by single crystal X-ray diffraction and depiction of important angles α, β and γ with values [in deg] for **3**: 173.82(5), 153.17(9), 12.58(19); for **6**: 173.43(9), 165.43(11), 0.4(3); for **7**: 178.75(7), 174.6(1), 24.3(2); for **8**: 176.84(9), 167.01(10), 21.4(2).

carbene complexes. Thus, the degree of flexibility facilitated by the environment should greatly influence the electronic communication between the donor and acceptor ligand and, consequently, the excited state behavior of the CT states.

Photophysical Studies

The UV/vis absorption spectra of the chiral copper(I) carbazolate complexes **1**–**4** and **6**–**8** in THF are very similar to those of previously reported structurally related CMAs and show intense high energy MLCT and ππ* transitions of the *N*-Dipp substituent between $\lambda = 250$–320 nm (Figure 2, Figure S15).[16,19] The vibrationally resolved band at $\lambda = 320$–375 nm ($\varepsilon = 5$–$8 \cdot 10^3$ $M^{-1}cm^{-1}$) is typical for LC(ππ*) states of the Cbz-type ligands (Figure 3). A very broad and moderately intense ($\varepsilon = 4$–$6 \cdot 10^3$ $M^{-1}cm^{-1}$) low energy absorption, with λ_{max} varying between 370–400 nm in dependence of the Cbz substitution and overlapping with the LC(Cbz) band, can be assigned to the S_0γS_1 transition of dominantly LL(Cbz→cAAC)CT character with some ML(Cu→cAAC)CT admixture according to our TD-DFT calculations (Figures 3 and S17). The $S_0 \rightarrow S_1$ transition of [Cu(PZN)(cAAC^{Ment})] (**6**), which we conclude to be LL(PZN→cAAC)/MLCT in nature, is also very broad but significantly bathochromically shifted to $\lambda_{max} = 475$ nm. In contrast to the Cbz localized ππ* bands, the LC(PZN) band at $\lambda_{max} = 350$ nm is broad and apparently contains an intraligand (IL)CT contribution.

The carbazolate compounds **1**–**4**, **7** and **8** exhibit bright green luminescence in THF at room temperature with a broad spectral appearance indicative of LLCT states (Table 1 and Supporting Information). The combination of moderate to high quantum yields $\varphi = 0.36$–0.88 and high radiative rate constants k_r of ca. 3–$4 \cdot 10^5$ s^{-1} are the result of an efficient TADF process as described by Thompson et al. for structurally related copper(I) complexes, and is highly environment sensitive.[16] In general, the emission wavelengths found in flexible polar media undergo a hypsochromic shift in rigid polar matrices, for example microcrystalline solid state or PMMA, as depicted in Figure 4 for [Cu(*Cbz^{Me})(cAAC^{Me})] (**8**) (see also Table 1 and Supporting Information). Interestingly, upon grinding the crystalline material, the emission again shifts bathochromically.

Theoretical work by Marian et al. suggests that the ground state S_0 of CMAs is more polar than the LLCT excited state and the respective static electric dipole moments point in opposite directions.[16,17,23] Since a rigid polar environment cannot reorganize to acknowledge the new dipole moment of the excited species, the $^{1/3}$LLCT states are then more destabilized than in fluxional media and thus higher emission energies are observed. The emission in polar THF solution, which can readjust its dipole orientation on the timescale of the excited state lifetime, is further shifted bathochromically due to destabilization of the ground state at the reorganized LLCT geometry and its environment within the Franck-Condon principle. In contrast, the $^{1/3}$LLCT states of the Cu^{I} complexes in the ground samples experience a smaller destabilization by the environment, i.e. the surrounding complex molecules that remain in their S_0 state. We attribute this finding to partial disruption of the crystalline order and a larger surface-to-volume ratio upon grinding, increasing the number of surface molecules that influence the photophysical properties of the macroscopic sample. Both effects decrease the destabilizing influence of the dipole-dipole interactions mentioned above, and thus give rise to a bathochromic shift compared to the single crystalline solid state.

In other media than THF, the chiral copper(I) complexes **2**–**4**, **8** and racemic **7** show higher k_r in comparison to [Cu(Cbz)(cAAC^{Ment})] (**1**), which can vary by two orders of magnitude between 10^3–10^5 s^{-1} at room temperature in dependence of the environment, with a record within this series of $k_r = 5.1 \cdot 10^5$ s^{-1} resulting in $\varphi = 0.91$ for [Cu(Cbz^{tBu})(cAAC^{Ment})] (**4**) in the ground solid. The substitution patterns at the *N*-donor ligand also lead to significantly higher rate constants for non-radiative decay k_{nr} on the order of 10^5 s^{-1}, giving quite diverse φ between 0.01–0.91 (Table 1).

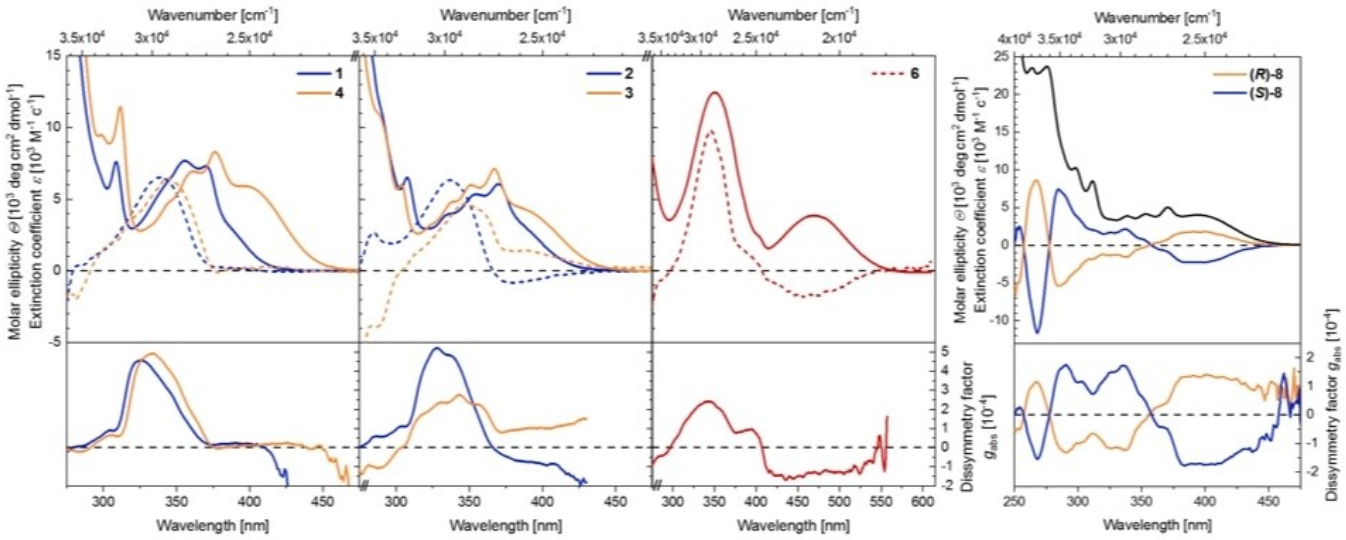

Figure 2. Absorption (solid) and ECD (dashed) spectra of **1**–**4**, **6** and (***S/R***)-**8** recorded in THF (c = 10^{-5}–10^{-4} mol L^{-1}) at room temperature.

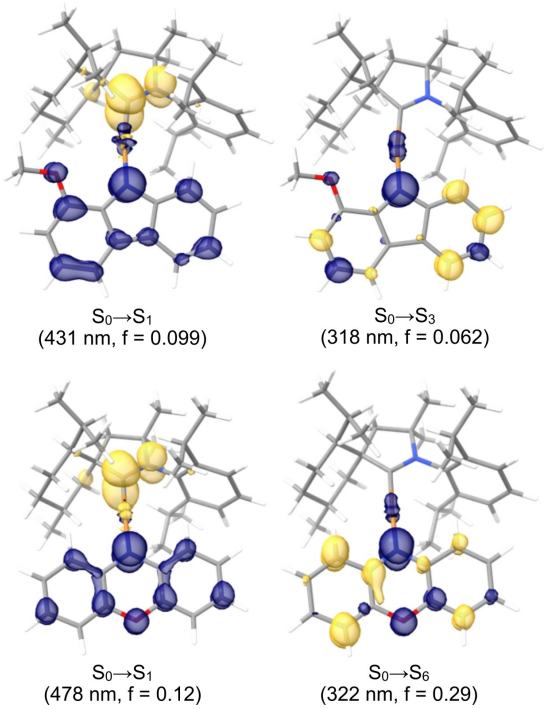

Figure 3. Selected electron density differences (isovalue ±0.005) relevant for the experimental absorption spectra of **3** (top) and **6** (bottom) in THF calculated at the D3(BJ)-PBE0/ZORA/def2-SVP level of theory. Loss of electron density is indicated in blue and gain in yellow.

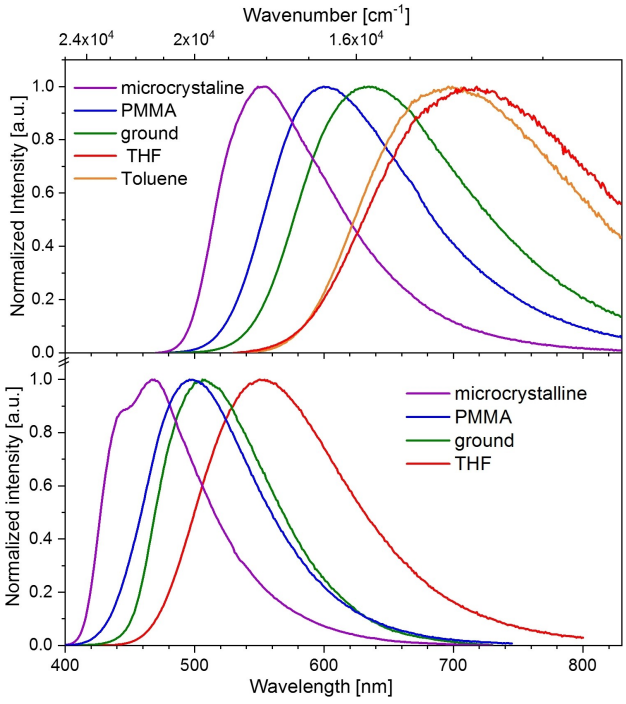

Figure 4. Normalized emission spectra of **6** (top) and **8** (bottom) in various media under argon at room temperature.

The changes in k_r and k_{nr}, and thus in φ, do not follow any obvious trend but rather seem to be the result of a combination of various effects. While free rotation and other reorganisation processes of the Cbz ligand allow for facile ISC and rISC that are paramount for efficient TADF, rigidification can hamper this mechanism.[22] Furthermore, the polarity of the environment has a large influence on the energy gap between the LLCT and LC states, which determines on the one hand the nature of the emitting states, but on the other hand the operative SOC and thus the efficiency of spin-forbidden processes.[29] We also note that the copper(I) carbazolate complexes experience diverse specific environments in the single crystalline solid state because of their different space groups, which also influence the respective dipole interactions between the complex molecules. As a result, these combined parameters can even switch the emission from TADF to dominantly phosphorescence from the ^{3}LLCT state with weak SOC as is evident from the broad spectral appearance and low k_r of **2** ($4.9 \cdot 10^4$ s^{-1}) and **3**

Table 1. Selected photophysical data of the chiral copper(I) complexes **1**–**4** and **6**–**8** recorded in the solid state at room temperature. For biexponential lifetime decays, the relative pre-exponential factors are given in parentheses.

	Medium	λ_{em} [nm]	τ [µs]	φ[a]	k_r [10^4 s^{-1}]	k_{nr} [10^4 s^{-1}]		Medium	λ_{em} [nm]	τ [µs]	φ[a]	k_r [10^4 s^{-1}]	k_{nr} [10^4 s^{-1}]
1	THF	509	2.7	0.88	32	4.4	**6**	THF	715	0.032	0.01	31	3069
	Crystal	466	25.6 (72)/ 86.4 (28)	0.12	0.28	2.1		Toluene	698	0.048	0.01	21	2079
	Ground	492	4.8 (90)/ 34.2 (10)	0.44	5.6	7.1		Crystal	553	0.26 (12)/1.0 (88)	0.72	79	31
	PMMA	472	6.8 (90)/ 31.5 (10)	0.53	5.8	5.1		Ground	635	0.09 (46)/0.25 (54)	0.12	70	513
2	THF	537	1.5	0.47	31	35		PMMA	601	0.16 (20)/0.53 (60)/1.0 (20)	0.29	67	164
	Crystal	476	2.3 (76)/5.6 (24)	0.15	4.9	28	**7**	THF	530	1.6	0.52	33	30
	Ground	503	1.5 (95)/4.1 (5)	0.37	23	39		Crystal	440	1.1 (76)/2.3 (24)	0.27	20	54
	PMMA	485	1.0 (93)/7.1 (7)	0.39	26	41		Ground	490	1.8	0.45	25	31
3	THF	540	0.86	0.38	44	72	**8**	THF	550	1.3	0.36	28	50
	Crystal	490	2.1 (88)/4.8 (12)	0.01	0.41	41		Crystal	470	2.1 (76)/4.1 (24)	0.33	11	22
	Ground	513	1.9 (91)/5.5 (9)	0.21	9.3	35		Ground	505	1.9	0.63	33	19
	PMMA	484	2.2 (90)/7.2 (11)	0.65	24	13		PMMA	498	1.8 (84)/4.8 (16)	0.13	5.7	38
4	THF	537	1.8	0.65	36	19							
	Ground	519	1.8	0.91	51	5.0							
	PMMA	485	3.2 (90)/ 15.7 (10)	0.13	2.9	19							

[a] Error margin ±0.02.

($4.1 \cdot 10^3$ s^{-1}) in crystalline samples, or **4** ($2.9 \cdot 10^4$ s^{-1}) and **8** ($5.7 \cdot 10^4$ s^{-1}) in PMMA.

Shifting the $^{1/3}$LLCT states to lower energy by introduction of a stronger *N*-donor in [Cu(PZN)(cAAC^{Ment})] (**6**) gives rise to efficient TADF in rigid environments, with very high k_r of up to $7.9 \cdot 10^5$ s^{-1} and concomitant $\varphi = 0.79$ in crystalline material (Table 1). We note that previously reported [Cu(PZN)(cAAC^{Ad})] is too weak an emitter for determination of k_r, while its heavier congener [Au(PZN)(cAAC^{Ad})] exhibits k_r of only 0.4–$2.2 \cdot 10^5$ s^{-1}.[18] As such, **6** is in general amongst the most efficient copper(I)-based triplet exciton emitters and even rivals the k_r of structurally related gold(I) cAAC amides, underlining the potential of earth abundant 3d elements for photoactive materials. Increasing λ_{max} from 553 nm in the single crystals to 601 and 635 nm in PMMA and the ground material, respectively, leads to more pronounced non-radiative decay and $\varphi =$ 0.12 as a result of Siebrand's rule, which states that vibrational overlap and k_{nr} increase with decreasing energy gap between the excited state and the ground state.[30] The bathochromic shift even in rigid environments is much more severe for **6** than observed for the other investigated CMA compounds.

In solution, the emission shifts even further to lower energies with emission maxima at 698 and 735 nm in toluene and THF, respectively. High k_r of $2–3 \cdot 10^5$ s^{-1} typical for TADF are maintained, but the energy-gap law and increased structural flexibility leads to enhanced radiationless deactivation of the excited states.

Chiroptical Analysis

The chiral copper(I) complexes described above feature efficient TADF in THF solution from the lowest energy ^{1}LLCT state. In this scenario, we expect the measured dissymmetry of the lowest energy absorption band g_{abs} (Eq. (2)) to be of the same order of magnitude as the g_{lum} of the triplet exciton emission.[31] Therefore, we first analyzed the circular dichroism of the $S_0 \rightarrow S_1$ transition to relate the chiroptical properties to the structural peculiarities of the ground state (Figure 2 and Supporting Information). Important data obtained from Eqs. 1 and 2 that connect the measured dissymmetry with the electronic ($\vec{\mu}$) and magnetic ($\vec{m}$) transition dipole moments, and the angle θ between their vectors, are given in Table 2.

$$g_{abs} = \frac{\Delta\varepsilon}{\varepsilon} = \frac{\varepsilon_L - \varepsilon_R}{\frac{1}{2}(\varepsilon_L + \varepsilon_R)} \quad (2)$$

Table 2. Chiroptical properties of the $S_0 \rightarrow S_1$ transition of **1**–**4**, **6** and (***S/R***)-**8** in THF solution.

	λ_{max} [nm]	ε [$M^{-1}cm^{-1}$]	FWHM [cm^{-1}]	f	$\lvert\vec{\mu}\rvert$ [D]	g_{abs} [10^{-4}]	$\lvert\vec{m}\rvert\cos(\theta)$[$10^{-3}$ μ_B]
1	370[a]	4500[a]	3200[a]	0.061	2.2	0.2	1
2	375[a]	4000[a]	3200[a]	0.055	2.1	0.9	5
3	385[a]	4600[a]	3500[a]	0.070	2.4	−1.0	6.4
4	395	5900	3600[a]	0.091	2.8	0.1	0.7
6	470	3850	3600	0.059	2.4	−1.0	6.6
(***S***)-**8**	395	4000	3600	0.061	2.3	−1.7	10
(***R***)-**8**	395	4000	3600	0.061	2.3	1.4	8.6

[a] Data approximated due to partial overlap of the $S_0 \rightarrow S_1$ transition with the absorption band of the LC($\pi\pi^*$) state of the Cbz ligand.

The g_{abs} values increase by ca. one order of magnitude from $2 \cdot 10^{-5}$ and $1 \cdot 10^{-5}$ for **1** and **4** with symmetric carbazolate ligands, respectively, to $9 \cdot 10^{-5}$ and $1.0 \cdot 10^{-4}$ for compounds **2** and **3** bearing asymmetric carbazolates. For the (***R/S***)-enantiomers of **8** we find g_{abs} of $1.4 \cdot 10^{-4}$ and $-1.7 \cdot 10^{-4}$, respectively, while the LLCT band of the PZN compound **6** at 475 nm exhibits $g_{abs} = 1.0 \cdot 10^{-4}$. Surprisingly, there seems to be no direct correlation between ε_{max} of the LLCT band and its g_{abs} value, implying that either $\lvert\vec{m}\rvert$ or $\cos(\theta)$ also varies. Since the oscillator strength f can be obtained from the experimental data and is directly related to the electronic transition dipole moment $\lvert\vec{\mu}\rvert$ via

$$f_{1,0} = \frac{4\varepsilon_0 \cdot m_e \cdot c^2 \cdot \ln(10)}{N_A \cdot e^2} \cdot \int \varepsilon(\tilde{\nu}) d\tilde{\nu} = \frac{8\pi^2 \cdot m_e \cdot c}{3h \cdot e^2} \cdot \tilde{\nu}_{max} \cdot \mu^2_{1\leftarrow 0} \quad (3)$$

with the integrated transition intensity being approximated by $\pi/2 \cdot \varepsilon_{max} \cdot \Gamma$ (Γ = full width at half maximum),[32] we could estimate the product of $\lvert\vec{m}\rvert\cos(\theta)$ using Equation (1).

While f and $\lvert\vec{\mu}\rvert$ for our complexes are in line with earlier published data ($f \approx 0.1$ and $\lvert\vec{\mu}\rvert \approx 3$ D) obtained from QC calculations,[16] the values of $\lvert\vec{m}\rvert\cos(\theta)$ vary greatly from only $0.7 \cdot 10^{-3}\,\mu_B$ for **4** to $10 \cdot 10^{-3}\,\mu_B$ for **8**. It is reasonable to assume that the decreased "kink" angle β or the increased torsion angle γ between the amide and carbene ligands are generally responsible for enhancing $\lvert\vec{m}\rvert\cos(\theta)$ as the PZN ligand and substitution in the 1-position of the Cbz are obviously advantageous for the dissymmetry. Since $\cos(\theta) < 1$, the minimum value we deduce for $\lvert\vec{m}\rvert\cos(\theta)$ of the ^{1}LLCT is $6.6 \cdot 10^{-3}\,\mu_B$, which is relatively small compared to, for example, f-f* transitions in lanthanide complexes ($\lvert\vec{m}\rvert\cos(\theta) \approx 0.2\,\mu_B$) or the absorption in chiral knot copper(I) complexes reported by Meskers and co-workers ($\lvert\vec{m}\rvert \approx 0.5\mu_B$).[33,34] However, we note that on the one hand the structural flexibility in solution can have a drastic effect on the relative orientation of $\vec{\mu}$ and $\vec{m}$, but on the other hand it also allows for beneficial high k_r (see above).[17,23]

Studies on the circularly polarized triplet emission of copper(I) complexes are scarce and recently, linearly coordinated C_1-symmetric [CuCl(cAAC^{Ment})] has been reported by Ung et al. to show $g_{lum} = 1.3 \cdot 10^{-3}$ for yellow luminescence with $\lambda_{max} = 555$ nm and $\varphi = 0.018$ in THF solution.[35] In order to ensure comparability of data, we reinvestigated that compound with our instrumental set-up and obtained dissymmetry values for the absorption of $g_{abs} = 2.6 \cdot 10^{-3}$ (Figure S13), similar to the data we extract from the $\Delta\varepsilon$ and ε plots given in the Supporting Information of Ung et al. of $3.4 \cdot 10^{-3}$. Also, the dissymmetry values for the emission at concentrations of $1–4 \cdot 10^{-4}$ M could be confirmed. However, a significant hypsochromic shift of the emission to $\lambda_{max} = 450$ nm is observed in PMMA and in the solid state that is more in line with our own studies on structurally related [CuX(cAAC^{Me})] complexes, arguing for excimer formation in solution (Figure 5).[26]

Indeed, the quantum yields are enhanced to 0.12 upon increasing the concentration to $4 \cdot 10^{-4}$ M, which suggests reduced non-radiative decay due to higher rigidity of the excited state. Furthermore, Thompson et al. have previously demonstrated that copper(I) cAAC halide complexes are prone to excimer and exciplex formation in non-coordinating and coordinating solvents, respectively, leading to severe bath-

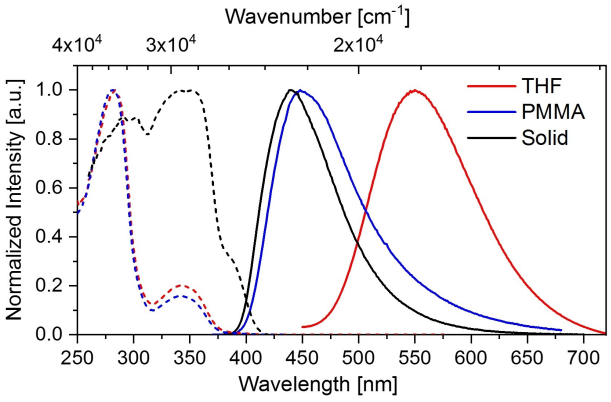

Figure 5. Normalized excitation (dashed) and emission (solid) spectra of [CuCl(cAAC^{Ment})] in THF, PMMA and in the solid state at room temperature, indicating excimer formation in solution.

ochromic shifts from blueish-green to orange, which is hindered in rigid matrices.[36] Since [CuCl(cAAC^{Ment})] shows identical emission spectra and g_{lum} in concentrated benzene and in THF solutions ($5\cdot10^{-3}$ M),[37] we thus conclude that the CPL detected for [CuCl(cAAC^{Ment})] most likely originates from a dimeric species with a {Cu(μ-Cl)$_2$Cu} core, i.e. trigonally coordinated Cu^{I} ions, and not linearly coordinated monomers.

We were therefore curious to study the CPL properties of our linearly coordinated copper(I) amide compounds, but unfortunately the g_{lum} of the Cbz complexes in THF solution as well as in PMMA matrices is below the detection limit of our instrument ($<1\cdot10^{-3}$). Actually, this finding coincides with the obtained low values for g_{abs} of the ^{1}LLCT states, which are responsible for the TADF process (Table 2). In contrast, and counterintuitively, [Cu(PZN)(cAAC^{Ment})] (**6**) exhibits $g_{lum} = -3.4\cdot10^{-3}$ for triplet exciton emission in PMMA (1–2.5 wt.%) (Figure 6), but not in other media. Optical artefacts, which might derive from linear dichroism and birefringence, were further excluded by measurement at several angles and positions of the films. It is important to note that the CPL of [Cu(PZN)(cAAC^{Ment})] (**6**) is similar to other chiral organic TADF emitters,[38] but combines the relatively high dissymmetry with higher k_r of nearly $7\cdot10^5$ s^{-1} in the red region of the electromagnetic spectrum (Table 1). Furthermore, the circular polarisation brightness $B_{CPL} = \varepsilon\cdot\varphi\cdot g_{lum}/2$ of 1.9 M^{-1}cm^{-1} is similar to other CPL emitting materials, and even better than obtained for most Ir^{III}- and Pt^{II}-based triplet emitters featuring comparable k_r,[39] highlighting the potential of linearly coordinated copper(I) TADF emitters for this purpose.

The origin of the CPL performance of **6** in comparison to the other CMA compounds must be related to the specific excited state structure and coupling with energetically higher lying states, which should depend on the limited geometrical reorganisation in PMMA as a rigid polar environment (see above). This can be concluded from the fact that CD measurements of **6** in PMMA films provide g_{abs} similar to those in THF ($1.0\cdot10^{-4}$), and one order of magnitude smaller than the g_{lum},

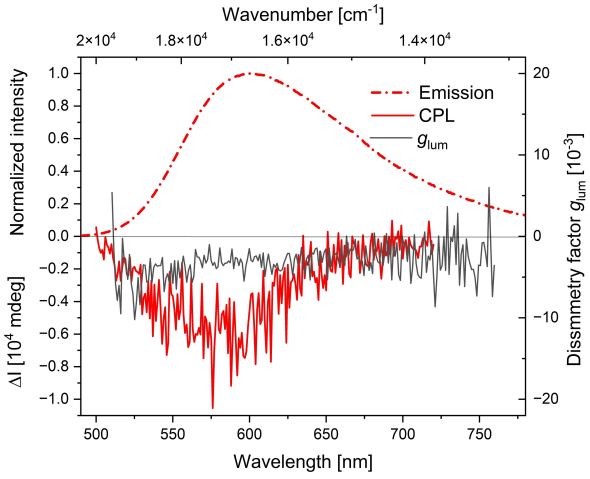

Figure 6. Normalized emission spectrum (dotted red), CPL spectrum (solid red) and corresponding g_{lum} values (grey) of [Cu(PZN)(cAAC^{Ment})] (**6**) in PMMA at room temperature.

which suggests negligible rotatory strength R of the ^{1}LL(PZN→cAAC^{Ment})CT transition at the ground state geometry. In addition, a "chaotic" reorganisation process is indicated by the three lifetime components necessary to fit the time-resolved luminescence decay. The increasing g_{lum} observed at higher emission energies ($5\cdot10^{-3}$ at 520 nm) indicates that more destabilized and less reorganised conformations exhibit enhanced R.

If indeed the reduced reorganisation in PMMA is responsible for the high g_{lum}, it does not at the same time decrease k_r significantly in comparison to other media (see Table 1). This beneficial result might be due to one of the following two extreme scenarios within the TADF scheme or, more likely, a combination of both: 1) as $g_{lum}{}^2$ scales with $k_F{}^{-1}$, a higher k_{RISC} might compensate a decreased oscillator strength $f(S_1\rightarrow S_0)$, or 2) the product $\left|\vec{m}\right|\cos(\theta)$ is increased. Assuming for the first case $k_{RISC} \gg k_F$, and therefore $k_r \approx k_F$, a maximum possible value of $\left|\vec{m}\right|\cos(\theta) = 0.046\ \mu_B$ for $S_1\rightarrow S_0$ is obtained using Eqs. 1 and 3, with $k_F = 6.7\cdot10^5$ s^{-1} and $\tilde{\nu}_{max} = 19{,}000$ cm^{-1} providing $f = 0.0022$ and $\left|\vec{\mu}\right| = 0.50$ D for the ^{1}LLCT emission. Regarding the second possibility, we use $\left|\vec{\mu}\right| = 2.4$ D of the $S_0\rightarrow S_1$ absorption band, which then yields $f = 0.05$, and Equation (1) with $|g_{lum}| = 0.0034$ provides a magnetic transition dipole moment of $\left|\vec{m}\right|\cos(\theta) = 0.22\ \mu_B$. In both extreme cases, i.e. either minimized $k_r(S_1\rightarrow S_0)$ or maximized $\left|\vec{m}\right|\cos(\theta)$, the latter is greatly increased in comparison to the estimated value of the absorption process of 0.0066 μ_B (see above). This result appears indeed realistic, in particular if $\cos(\theta)\approx1$, considering that for a similarly sized [Cu(phen)$_2$]$^+$ complex a value of 0.5 μ_B was found for $\left|\vec{m}\right|$.[34]

Large differences between the dissymmetry values g in solution and rigid media are often explained with aggregation or excimer formation of emitter molecules.[40] These effects have been described in detail to be of importance for planar Pt^{II} complexes and extended (organic) π-systems, and can lead to greatly enhanced g_{lum}.[12] An interesting behavior was also reported by Wang et al. for highly ordered assemblies of a non-planar phosphorescent Cu^{I} complex, showing negligible CPL in DMSO suspension, but increasing g_{lum} values of $5\cdot10^{-3}$ for films and $1\cdot10^{-2}$ for microcrystalline solid state.[41] A similar behavior was also found for aggregated chiral NHC copper(I) amide complexes.[24] However, for [Cu(PZN)(cAAC^{Ment})] (**6**) we exclude excimer formation or aggregation being responsible for the remarkable g_{lum} in PMMA due to the low concentration of the dopant of 1 to 2.5 wt.%, and the emission and excitation parameters do not show typical signs for such processes.

Besides restricted reorganisation in PMMA, either a butterfly or a "kink" angle distortion of the PZN ligand in the excited state can also provide a mechanism to enhance the rotatory strength of the transition. A butterfly distortion of the more rigid Cbz ligands in **1**–**4**, **7** and **8** would be hindered, while the excited state structure in CMAs is typically coplanar,[17,23] which could thus further explain the inefficiency of CPL in such compounds. Also, the polar matrix PMMA could support distortions by hydrogen bonding to the oxygen of the PZN

ligand, an interaction mechanism that would also not be available for the Cbz ligands.

An indication of a possible environment dependent distortion is provided by our DFT/TD-DFT calculations on **6** in the gas phase, showing that the rotatory strength *R* of the vertical transitions between the ground state S_0 and the S_1 state are very structure sensitive (Figure 7).

The lowest energy conformation of the S_0 state adopts a nearly coplanar arrangement of the phenoxazine and cAAC^{Ment} ligands and bears very little rotatory strength *R* in the vertical transition $S_0 \rightarrow S_1$ (Figure 7), which is in line with the measured CD spectra in solution (Figure 2 and Table 2). Interestingly, we found a "kink" angle β distortion of **6** as a local minimum on the energy potential surface of the ground state only 0.03 eV above the planar geometry, which is thus thermally accesible at room temperature. The vertical transition to the S_1 state then exhibits a ten-fold increased *R* value of $10.2 \cdot 10^{-40}$ cgs. Furthermore, the mathematical sign of the luminescence dissymmetry is also very sensitive to the structural pecularities, since the $S_0 \rightleftharpoons S_1$ transition at the optimized T_1 geometry, which ist most likely very relevant for the TADF process, shows $R = -7.5 \cdot 10^{-40}$ cgs.

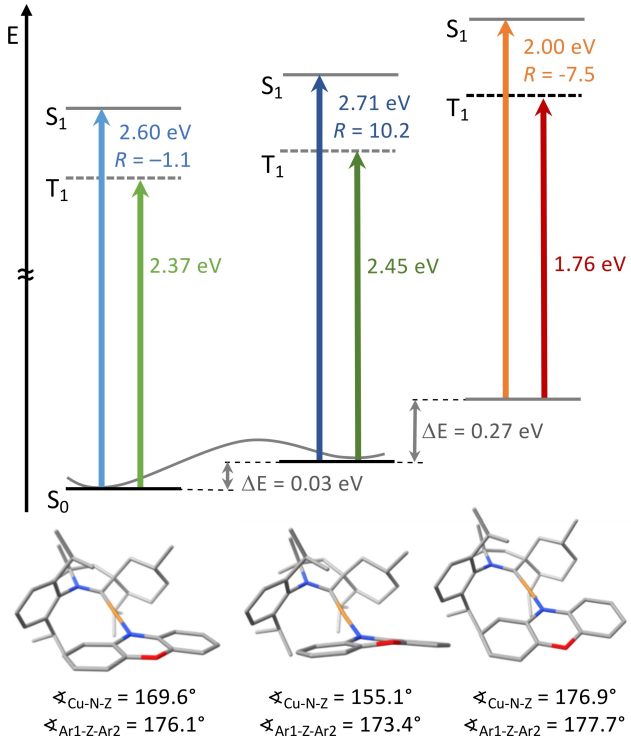

Figure 7. TD-DFT (D3BJ-PBE0/ZORA/def2-SVP) calculated vertical transitions of [Cu(PZN)(cAAC^{Ment})] (**6**) from the DFT (D3BJ-PBE0/ZORA/def2-TZVP) optimized geometries of the ground state S_0 (left and middle), and from S_0 at the optimized T_1 geometry (right). Z denotes the centroid of the amide ligand, while Ar1 and Ar2 denote their two arene rings. Rotatory strengths *R* given in 10^{-40} cgs.

Conclusions

Structure-property relationships for the design of chiroptical properties of transition metal CP-TADF emitters are very scarce despite their relevance for electroluminescent devices. We have thus studied a series of chiral copper(I) carbene amide complexes as representatives of a class of highly efficient TADF emitters, which emit from $^{1/3}$LLCT/MLCT states with high k_r in the range of 10^5 s^{-1} at room temperature as reported previously for non-chiral or racemic analogues. For all compounds, pronounced mechanochromic photoluminescence behavior upon grinding the single crystalline materials leading to bathochromic emission shifts and increased k_r is observed. We trace this phenomenon back to changes in the intermolecular dipol-dipol interactions and larger surface-to-volume ratio after application of the stimulus. However, the chiral moieties at the cAAC acceptor or amide donor ligand do not lead to detectable CPL of the carbazolate complexes irrespective of the medium.

In contrast, [Cu(PZN)(cAAC^{Ment})] (**6**) is a very efficient orange-red TADF emitter in PMMA ($k_r = 6.7 \cdot 10^5$ s^{-1}) with a notable dissymmetry factor of $g_{lum} = -3.4 \cdot 10^{-3}$. Either restricted ligand rotation or a "kink" angle distortion of the PZN ligand supported by hydrogen bonding of the ligand's oxygen atom with the PMMA matrix might be responsbile for producing the rotatory strength of the electron density change of the vertical transition. Such an interaction with the matrix is not available to the carbazolate ligands and is thus most likely responsible for the effective chiroptical properties of the excited states, which are inherently introduced by the chiral carbene ligand. Further exploitation of this design motif for efficient CP-TADF is a currently ongoing work in our group and will be reported in due course.

Experimental Section

Essential Experimental Procedures/Data.All experimental details provided in the Supporting Information in a separate file (pdf), including synthetic procedures, details of characterization, X-ray crystallographic data, photophysical spectra, as well as computational details.

Deposition Number(s) 2175343 (for **3**), 2195861 (for **6**), 2195860 (for **7**), 2175342 (for ***R*-8**), 2175341 (for ***S*-8**) contain(s) the supplementary crystallographic data for this paper. These data are provided free of charge by the joint Cambridge Crystallographic Data Centre and Fachinformationszentrum Karlsruhe Access Structures service.

Acknowledgements

Financial support by the Deutsche Forschungsgemeinschaft (DFG STE1834/4-2) is gratefully acknowledged. This work was funded by the Deutsche Forschungsgemeinschaft (DFG, German Research Foundation) under Germany's Excellence Strategy EXC2033, project number 390677874, RESOLV. The authors gratefully acknowledge the computing time provided on the Linux HPC cluster at Technical University Dortmund (LiDO3), partially funded in the course of the Large-Scale Equipment

Initiative by the German Research Foundation (DFG) as project 271512359. Open Access funding enabled and organized by Projekt DEAL.

Conflict of Interests

The authors declare no conflict of interest.

Data Availability Statement

The data that support the findings of this study are available in the supplementary material of this article.

Keywords: chirality · circularly polarized luminescence · copper · excited states · TADF

[1] C. Wagenknecht, C.-M. Li, A. Reingruber, X.-H. Bao, A. Goebel, Y.-A. Chen, Q. Zhang, K. Chen, J.-W. Pan, *Nat. Photonics* **2010**, *4*, 549–552.
[2] C. H. Bennett, G. Brassard, *Theor. Comput. Sci.* **2014**, *560*, 7–11.
[3] R. Farshchi, M. Ramsteiner, J. Herfort, A. Tahraoui, H. T. Grahn, *Appl. Phys. Lett.* **2011**, *98*, 162508.
[4] S. J. Bradberry, A. J. Savyasachi, M. Martinez-Calvo, T. Gunnlaugsson, *Coord. Chem. Rev.* **2014**, *273–274*, 226–241.
[5] G. Muller, *Dalton Trans.* **2009**, *44*, 9692–9707.
[6] M. Schadt, *Annu. Rev. Mater. Sci.* **1997**, *27*, 305–379.
[7] a) L. Rosenfeld, *Z. Phys.* **1929**, *52*, 161–174; b) J. A. Schellman, *Chem. Rev.* **1975**, *75*, 323–331.
[8] a) F. Zinna, L. Di Bari, *Chirality* **2015**, *27*, 1–13; b) T. Harada, H. Tsumatori, K. Nishiyama, J. Yuasa, Y. Hasegawa, T. Kawai, *Inorg. Chem.* **2012**, *51*, 6476–6485.
[9] J.-R. Jiménez, B. Doistau, C. M. Cruz, C. Besnard, J. M. Cuerva, A. G. Campaña, C. Piguet, *J. Am. Chem. Soc.* **2019**, *141*, 13244–13252.
[10] C. Murawski, K. Leo, M. C. Gather, *Adv. Mater.* **2013**, *25*, 6801–6827.
[11] a) E. Zysman-Colman, (Hrsg.) *Iridium (III). In optoelectronic and photonics applications*, John Wiley & Sons Inc, Chichester, West Sussex, **2017**; b) G. Hong, X. Gan, C. Leonhardt, Z. Zhang, J. Seibert, J. M. Busch, S. Bräse, *Adv. Mater.* **2021**, *33*, e2005630.
[12] B. Doistau, J.-R. Jiménez, C. Piguet, *Front. Chem.* **2020**, *8*, 555.
[13] C. Shen, E. Anger, M. Srebro, N. Vanthuyne, K. K. Deol, T. D. Jefferson, G. Muller, J. A. Gareth Williams, L. Toupet, C. Roussel, J. Autschbach, R. Réau, J. Crassous, *Chem. Sci.* **2014**, *5*, 1915–1927.
[14] L. Frédéric, A. Desmarchelier, L. Favereau, G. Pieters, *Adv. Funct. Mater.* **2021**, *31*, 2010281.
[15] Z.-L. Tu, Z.-P. Yan, X. Liang, L. Chen, Z.-G. Wu, Y. Wang, Y.-X. Zheng, J.-L. Zuo, Y. Pan, *Adv. Sci.* **2020**, *7*, 2000804.
[16] R. Hamze, J. L. Peltier, D. Sylvinson, M. Jung, J. Cardenas, R. Haiges, M. Soleilhavoup, R. Jazzar, P. I. Djurovich, G. Bertrand, M. E. Thompson, *Science* **2019**, *363*, 601–606.
[17] M. Gernert, L. Balles-Wolf, F. Kerner, U. Müller, A. Schmiedel, M. Holzapfel, C. M. Marian, J. Pflaum, C. Lambert, A. Steffen, *J. Am. Chem. Soc.* **2020**, *142*, 8897–8909.
[18] A. S. Romanov, S. T. E. Jones, Q. Gu, P. J. Conaghan, B. H. Drummond, J. Feng, F. Chotard, L. Buizza, M. Foley, M. Linnolahti, D. Credgington, M. Bochmann, *Chem. Sci.* **2020**, *11*, 435–446.
[19] D. Di, A. S. Romanov, Le Yang, J. M. Richter, J. P. H. Rivett, S. Jones, T. H. Thomas, M. Abdi Jalebi, R. H. Friend, M. Linnolahti, M. Bochmann, D. Credgington, *Science* **2017**, *356*, 159–163.
[20] a) S. Shi, M. C. Jung, C. Coburn, A. Tadle, D. Sylvinson, P. I. Djurovich, S. R. Forrest, M. E. Thompson, *J. Am. Chem. Soc.* **2019**, *141*, 3576–3588; b) R. Tang, S. Xu, T.-L. Lam, G. Cheng, L. Du, Q. Wan, J. Yang, F.-F. Hung, K.-H. Low, D. L. Phillips, C.-M. Che, *Angew. Chem. Int. Ed.* **2022**, *61*, e202203982; c) A. Ruduss, B. Turovska, S. Belyakov, K. A. Stucere, A. Vembris, G. Baryshnikov, H. Ågren, J.-C. Lu, W.-H. Lin, C.-H. Chang, K. Traskovskis, *ACS Appl. Mater. Interfaces* **2022**, *14*, 15478–15493; d) A. Ying, Y.-H. Huang, C.-H. Lu, Z. Chen, W.-K. Lee, X. Zeng, T. Chen, X. Cao, C.-C. Wu, S. Gong, C. Yang, *ACS Appl. Mater. Interfaces* **2021**, *13*, 13478–13486; e) A. Ruduss, B. Turovska, S. Belyakov, K. A. Stucere, A. Vembris, K. Traskovskis, *Inorg. Chem.* **2022**, *61*, 2174–2185.
[21] M. J. Leitl, V. A. Krylova, P. I. Djurovich, M. E. Thompson, H. Yersin, *J. Am. Chem. Soc.* **2014**, *136*, 16032–16038.
[22] E. J. Taffet, Y. Olivier, F. Lam, D. Beljonne, G. D. Scholes, *J. Phys. Chem. Lett.* **2018**, *9*, 1620–1626.
[23] J. Föller, C. M. Marian, *J. Phys. Chem. Lett.* **2017**, *8*, 5643–5647.
[24] A. Ying, Y. Ai, C. Yang, S. Gong, *Angew. Chem. Int. Ed.* **2022**, *61*, e202210490.
[25] A. M. T. Muthig, O. Mrozek, T. Ferschke, M. Rödel, J. Kuhnt, C. Lenczyk, J. Pflaum, A. Steffen, *J. Am. Chem. Soc.* **2023**, *145*, 4438-4449.
[26] M. Gernert, U. Müller, M. Haehnel, J. Pflaum, A. Steffen, *Chem. Eur. J.* **2017**, *23*, 2206–2216.
[27] a) P. Roesch, J. Nitsch, M. Lutz, J. Wiecko, A. Steffen, C. Müller, *Inorg. Chem.* **2014**, *53*, 9855–9859; b) J. Nitsch, C. Kleeberg, R. Fröhlich, A. Steffen, *Dalton Trans.* **2015**, *44*, 6944–6960; c) P. Bissinger, A. Steffen, A. Vargas, R. D. Dewhurst, A. Damme, H. Braunschweig, *Angew. Chem. Int. Ed.* **2015**, *54*, 4362–4366; d) J. Nitsch, F. Lacemon, A. Lorbach, A. Eichhorn, F. Cisnetti, A. Steffen, *Chem. Commun.* **2016**, *52*, 2932–2935; e) B. Hupp, C. Schiller, C. Lenczyk, M. Stanoppi, K. Edkins, A. Lorbach, A. Steffen, *Inorg. Chem.* **2017**, *56*, 8996–9008; f) E. Hobbollahi, M. List, B. Hupp, F. Mohr, R. J. F. Berger, A. Steffen, U. Monkowius, *Dalton Trans.* **2017**, *46*, 3438–3442; g) H. Braunschweig, T. Dellermann, R. D. Dewhurst, B. Hupp, T. Kramer, J. D. Mattock, J. Mies, A. K. Phukan, A. Steffen, A. Vargas, *J. Am. Chem. Soc.* **2017**, *139*, 4887–4893; h) B. Hupp, J. Nitsch, T. Schmitt, R. Bertermann, K. Edkins, F. Hirsch, I. Fischer, M. Auth, A. Sperlich, A. Steffen, *Angew. Chem. Int. Ed.* **2018**, *57*, 13671–13675; i) N. V. Tzouras, E. A. Martynova, X. Ma, T. Scattolin, B. Hupp, H. Busen, M. Saab, Z. Zhang, L. Falivene, G. Pisanò, K. van Hecke, L. Cavallo, C. S. J. Cazin, A. Steffen, S. P. Nolan, *Chem. Eur. J.* **2021**, *27*, 11904–11911; j) A. Steffen, B. Hupp in *Comprehensive Coordination Chemistry III* (Ed.: E. Constable), Elsevier, San Diego, **2021**, pp. 466–502; k) T. Hölzel, A. Belyaev, M. Terzi, L. Stenzel, M. Gernert, C. M. Marian, A. Steffen, C. Ganter, *Inorg. Chem.* **2021**, *60*, 18529–18543; l) A. M. T. Muthig, M. Krumrein, J. Wieland, M. Gernert, F. Kerner, J. Pflaum, A. Steffen, *Inorg. Chem.* **2022**, *61*, 14833–14844; m) A. M. T. Muthig, J. Wieland, S. Koop, C. Lenczyk, F. Kerner, B. Hupp, A. Steffen, *Inorg. Chem.* **2022**, *61*, 17427–17437.
[28] a) A. Liske, L. Wallbaum, T. Hölzel, J. Föller, M. Gernert, B. Hupp, C. Ganter, C. M. Marian, A. Steffen, *Inorg. Chem.* **2019**, *58*, 5433–5445; b) J. Föller, C. Ganter, A. Steffen, C. M. Marian, *Inorg. Chem.* **2019**, *58*, 5446–5456.
[29] J. Feng, E. J. Taffet, A.-P. M. Reponen, A. S. Romanov, Y. Olivier, V. Lemaur, L. Yang, M. Linnolahti, M. Bochmann, D. Beljonne, D. Credgington, *Chem. Mater.* **2020**, *32*, 4743–4753.
[30] a) W. Siebrand, *Chem. Phys.* **1967**, *46*, 440–447; b) W. Siebrand, *Chem. Phys.* **1967**, *47*, 2411–2422.
[31] Y. Nagata, T. Mori, *Front. Chem.* **2020**, *8*, 448.
[32] P. Klán, J. Wirz, *Photochemistry of organic compounds. From concepts to practice*, Wiley, Chichester, **2009**.
[33] S. C. J. Meskers, *ChemPhotoChem* **2022**, *6*, e202100154.
[34] S. C. J. Meskers, H. P. J. M. Dekkers, G. Rapenne, J.-P. Sauvage, *Chem. Eur. J.* **2000**, *6*, 2129–2134.
[35] M. Deng, N. F. M. Mukthar, N. D. Schley, G. Ung, *Angew. Chem. Int. Ed.* **2020**, *59*, 1228–1231.
[36] a) A. S. Romanov, D. Di, Le Yang, J. Fernandez-Cestau, C. R. Becker, C. E. James, B. Zhu, M. Linnolahti, D. Credgington, M. Bochmann, *Chem. Commun.* **2016**, *52*, 6379–6382; b) R. Hamze, R. Jazzar, M. Soleilhavoup, P. I. Djurovich, G. Bertrand, M. E. Thompson, *Chem. Commun.* **2017**, *53*, 9008–9011.
[37] E. E. Braker, N. F. M. Mukthar, N. D. Schley, G. Ung, *ChemPhotoChem* **2021**, *5*, 902–905.
[38] a) M. Li, Y.-F. Wang, D. Zhang, L. Duan, C.-F. Chen, *Angew. Chem. Int. Ed.* **2020**, *59*, 3500–3504; b) S.-Y. Yang, Y.-K. Wang, C.-C. Peng, Z.-G. Wu, S. Yuan, Y.-J. Yu, H. Li, T.-T. Wang, H.-C. Li, Y.-X. Zheng, Z.-Q. Jiang, L.-S. Liao, *J. Am. Chem. Soc.* **2020**, *142*, 17756–17765.
[39] L. Arrico, L. Di Bari, F. Zinna, *Chem. Eur. J.* **2021**, *27*, 2920–2934.
[40] a) Y. Kitayama, T. Amako, N. Suzuki, M. Fujiki, Y. Imai, *Org. Biomol. Chem.* **2014**, *12*, 4342–4346; b) H. Tanaka, Y. Inoue, T. Mori, *ChemPhotoChem* **2018**, *2*, 386–402.
[41] J.-J. Wang, H.-T. Zhou, J.-N. Yang, L.-Z. Feng, J.-S. Yao, K.-H. Song, M.-M. Zhou, S. Jin, G. Zhang, H.-B. Yao, *J. Am. Chem. Soc.* **2021**, *143*, 10860–10864.

Research Article
doi.org/10.1002/chem.202300946

Manuscript received: March 24, 2023
Accepted manuscript online: June 5, 2023
Version of record online: August 11, 2023